Precision Engineering 84 (2023) 37–44

Contents lists available at ScienceDirect

Precision Engineering

journal homepage: www.elsevier.com/locate/precision

Constant probe orientation for fast contact-based inspection of 3D free-form surfaces using (3+2)-axis inspection machines☆

Oleksii Sliusarenko [b], Gaizka Gómez Escudero [a], Haizea González [a,*], Amaia Calleja [a], Michael Bartoň [b,c], Naiara Ortega [a], Luis Norberto López de Lacalle [a]

[a] High Performance Manufacturing Group, Department of Mechanical Engineering, the University of the Basque Country, Plaza Ingeniero Torres Quevedo 1, 48013, Bilbao, Basque Country, Spain
[b] BCAM – Basque Center for Applied Mathematics, Alameda de Mazarredo 14, 48009 Bilbao, Basque Country, Spain
[c] Ikerbasque – Basque Foundation for Sciences, Maria Diaz de Haro 3, 48013 Bilbao, Basque Country, Spain

ARTICLE INFO

Keywords:
Inspection path planning
(3+2)-axis inspection machine
Probe orientation optimization
Free-form surfaces

ABSTRACT

A new probe optimization method for contact based (3+2)-axis inspection machines is proposed. Given an inspection path of a stylus on a free-form surface, an optimal orientation of the stylus is computed such that (i) the inclination angle of the stylus is within a given angular range with respect to the surface normal, (ii) the motion of the stylus is globally collision free, and (iii) the stylus remains constant in the coordinate system of the measuring machine. The last condition guarantees that the inspection motion requires only the involvement of the three translational axes of the measuring machine. The numerical simulations were validated through physical experiments on a testcase of a tooth of a bevel gear due to the surface complexity and probe accessibility. This optimized method was compared to 3-axis and 5-axis inspection strategies, showing that the fixed (3+2)-axis stylus returns more accurate inspection results compared to the traditional 3-axis approach and similar to 5-axis approach.

1. Introduction & motivation

Fast and accurate inspection algorithms play a key role in any efficient manufacturing pipeline. The quality inspection process is typically realized by a coordinate measuring machine (CMM) that moves in space and measures the geometry of a 3D manufactured object by sensing a set of discrete points on its surface, see Fig. 1. Nowadays, there is a large number of types of optical and/or contact probes for 2D and/or 3D measurement that can be integrated into a CMM: tactile probes, vision systems, confocal microscopes, laser scanners, roughness probes, or interferometric probes, to name a few [1]. With multi-sensor CMMs, 100% of complex component features can be fully measured on a CMM without the need to move the part. However, the integration of the sensors requires a proper software that governs all of them, which is usually a challenge.

The laser and scanning-based approaches do not require physical contact with a to-be-inspected workpiece and the inspection machine, however, these approaches are more expensive, more demanding in terms of maintenance and have several more disadvantages, like (i) they show problems with shine surfaces (finishing machined surfaces); (ii) are less accurate than tactile systems when point-to-point is compared; (iii) cannot measure characteristics located where the light cannot access (in shadow or undercuts with respect to the light direction).

In contrast, tactile sensors are used in CMM from the very beginning and are the most popular inspection tools in industry. The inspection is achieved by a *touch probe*, that is composed by a ball (most often made of rubi, zirconia, silicon carbide, or diamond), a stylus (metallic, ceramic, or carbon fiber) and a stem (carbon fiber); the stem is sometimes telescopic to gain accessibility to inner zones of the workpiece. The probe moves in space and touches with the ball the manufactured workpiece at a set of 3D inspection points. The inspection machine can be controlled by a human operator, or *automatically* by a computer, navigated by a properly designed path-inspection algorithm.

The inspection machines can be categorized by the number of degrees of freedom (DoF) they possess. One of the CMMs configuration used in industry is (3+2) DoF inspection machine. Such a machine typically consists of a *bridge*, which is a large movable frame that

☆ This paper was recommended by Associate editor Prof. R. Leach.

* Corresponding author.
E-mail addresses: osliusarenko@bcamath.org (O. Sliusarenko), gaizka.gomez@ehu.eus (G.G. Escudero), haizea.gonzalez@ehu.eus (H. González), amaia.calleja@ehu.eus (A. Calleja), mbarton@bcamath.org (M. Bartoň), naiara.ortega@ehu.eus (N. Ortega), norberto.lzlacalle@ehu.eus (L.N.L. de Lacalle).

https://doi.org/10.1016/j.precisioneng.2023.06.013
Received 26 September 2022; Received in revised form 11 June 2023; Accepted 20 June 2023
Available online 27 June 2023

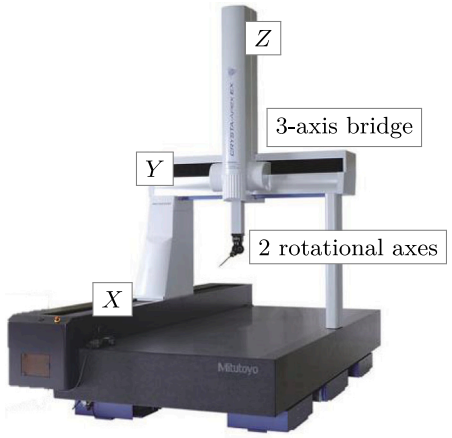

Fig. 1. A (3+2) contact-based inspection machine Mitutoyo Crysta Apex S-162012. The frame consists of 3 translational axes X, Y, and Z, and the orientation of the stylus is controlled by two additional rotational axes.

controls motions of three translational axes X, Y, and Z (3 DoFs), further provided with two rotational axes that control the rotation and inclination angles of the probe (another 2 DoFs), see Fig. 1. Since the linear axes of the CMM are much more precise than the rotational ones [2], one of the main objectives of any inspection process is to minimize the involvement of the two rotational axes. The proposed research belongs to the category of automatic contact-based approaches where the motion of the inspection probe is the unknown and one looks for an optimal orientation of the inspection stylus such that the inspection time is kept while improving the inspection quality.

The rest of the paper is organized as follows. Section 2 surveys the related research, Section 3 introduces the problem and the main objectives of the path-inspection algorithm and, in particular, Section 3.2 describes the computation of a set candidate directions and Section 3.3 discusses numerical computation including the selection of the best direction. The physical validations of the algorithm are shown in Section 4 and the conclusions are drawn in Section 5.

2. Previous work

The measurement of three-dimensional objects involves locating the section of space with the geometry of the object measured by means of a coordinate point in a coordinate system used as a reference. To carry out this location, CMMs have been considered a versatile system since 1956 when Ferranti developed the first machine [3]. Since then, this equipment has been further evolving, increasing its measurement capabilities with systems of a different nature.

Measurements of complex components in CMM typically require several DoFs of movement of the head along with the accessibility of the probe to the surface to be measured. The CMMs used in laboratories for these components typically have 4 or 5 axes for continuous measurement systems, normally with the rotary-linear-linear-linear (RLLL) kinematics in the first case and LLLRR in the latter one. However, according to the component to-be-measured geometry/dimensional requirements, from a financial point of view, a (3+2)-axis inspection machine could be selected instead of 5-axis, i.e., a 3-axis inspection machine provided by a tilting table with two degrees of freedom to position the to-be-inspected object. This reduction in the DoFs offers inspection trajectories that comply with accessibility restrictions.

CMM measurements of 3D free-form surfaces, and complex geometries, i.e. different types of rotary components such as blisk or gears, have been the subject of numerous studies [4–10]. Although tactile probes are still the most widely used at an industrial level, the metrological productivity of massive point acquisition systems based on optical systems is also gaining ground in these complex components. Vision systems [11] and, above all, laser scanner systems [12,13] are the solutions that are gaining strength due to their multiple subsequent applications based on obtaining the digital twin.

In the CAD/CAM literature, there are several relevant works inspection path-planning of curved geometries. [14–18]. An automatic sweep scan path planning system that generates a continuous sweep scanning path for the inspection of a free-form surface using a 5-axis CMM is presented in [14]. The two rotary axes have extremely low moment of inertia and the proposed method outperforms standard inspection algorithms, such as isoparametric or zigzag methods.

An isoparametric inspection method is introduced in [15]. The method proposes two sampling strategies, one called automatic, where the sampling points are selected using the deviation estimation between the inspected surface and the exact CAD model, and curvature-based sampling that aims at higher density of inspection points in regions that are highly curved. The simulations show favorable results when compared to an isoplanar inspection strategy, however, the method is parametrization-dependent, which may lead to different inspection results for the same geometries, just differently parameterized.

Given a CAD model of a to-be-inspected surface, a search-based planning algorithm is proposed to determine the locations of the sample curves extracted from the CAD model, selected automatically for inspection path planning [16]. The algorithm is validated using physical experiments on a variety of machined aircraft metal skins. An inspection method for free-form surfaces using a CMM equipped with a contact-based probe is introduced [17]. The proposed algorithm incorporates several steps that influence the quality of the inspection, namely: registration, definition of measurement points, probe path generation, path optimization and verification, and probe radius compensation. In terms of registration, a new registration algorithm is proposed that minimizes, in the least square sense, the deviation between the measured points and their counter parts on the nominal model.

An inspection path planning algorithm that looks for a discrete set of probe orientations is introduced in [18]. The unit sphere of the probe directions is sampled and the inspection points that can be approached by a single probe direction are grouped. The algorithm then looks for a minimum number of orientations from a given sampled set to guarantee that all inspection points can be accessed. The problem of finding the shortest inspection path is converted to the traveling salesman problem (TSP) and solved using heuristics methods. The algorithm is demonstrated on benchmark CAD geometries, including those containing cavities.

3. (3+2)-Axis contact-based inspection algorithm

The main aim is to perform a precision measurement of a machined 3D free-form surface using a (3+2)-axis contact-based CMM instead of the 5 continuous axes, commonly required for these type of complex surfaces ensuring the machining time and final measuring deviations. Since the inspection accuracy is correlated with the involvement of two rotational axes of the CMM, the main aim of this development consists on minimizing, or fully eliminating, if possible, inspection motions the involvement of the two rotational axes.

There are three main objectives on the direction d of the stylus for every inspection path:

1. *Inspection quality.* The inclination angle ϕ of the stylus in the *local* coordinate system stays within the range of 60°–75° w.r.t. the surface normal n at the contact point $c^{\perp}$, see Fig. 2 .
2. *Physical feasibility.* The motion of the probe is globally collision-free.
3. *Rotation elimination.* The inclination of the stylus remains constant in the coordinate system of the CMM.

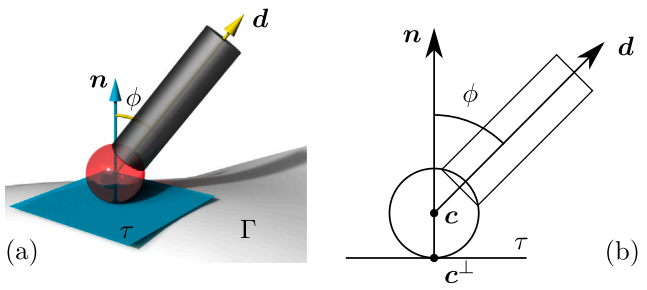

Fig. 2. Stylus inclination. The inclination of the stylus is measured by the angle ϕ between the stylus direction $\boldsymbol{d}$ and the surface normal $\boldsymbol{n}$ at the contact point $\boldsymbol{c}^{\perp}$ at the to-be-inspected surface Γ. τ is the tangent plane of Γ at $\boldsymbol{c}^{\perp}$. A 3D view (a) and a schematic 2D view (b) are shown.

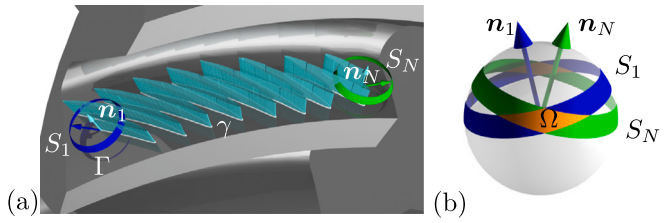

Fig. 3. (a) Surface normals of Γ along an inspection path γ (white) form as a ruled surface (cyan). The inspection path is discretized by $N = 2000$ inspection points. At the beginning and the end of the inspection path, two spherical strips are shown. These strips (blue and green) represent the admissible stylus directions at the boundary points of the inspection path. When mapped to a common unit sphere (b), the intersection of two spherical strips (orange patch) gives the stylus directions suitable simultaneously for both measurement points. (For interpretation of the references to color in this figure legend, the reader is referred to the web version of this article.)

Remark 1. The first requirement (Inspection quality) is specific to a particular measuring machine. For this purpose, a Mitutoyo Crysta Apex S-162012 CMM was used, with technical documentation recommended range of 60°–75° for the inclination angle ϕ such that the measuring process is the most reliable. In the presented computational framework, however, this range is a parameter and can be flexible changed in to be adapted to another CMM Machine.

3.1. Assumptions on the input geometry and measuring process

The aim is to perform a precision measurement of a machined 3D free-form surface with respect to its ideal (digital) model O. To this end, it is assumed in the simulations, and later on with physical validations, that a probe consists of a stylus model M2STY D2R L20 EWL14 D1.4SS from *Renishaw* (20 mm length, a ruby ball ⌀2 mm with a stainless steel ⌀1.4 mm stylus, see Fig. 7(a) and a stem model RSH 350 also from *Renishaw* (length 126.9 mm). For simplicity of the simulations, the geometry of the stem is disregarded under the assumption that the stylus is long enough (longer than the largest dimension of the model under inspection). If the stylus is closer and may collide with the inspected object, the algorithm is capable of using a bounding primitive (a box, sphere, or cylinder), that fully contains the stem and is easier for the global collision detection test.

The to-be-inspected object O is considered as a union of smooth (at least C^1-continuous) and oriented boundary surfaces, Γ_i, $i = 1, \dots, m$, connected in at least C^0-continuous fashion, which is a typical boundary representation (B-rep.) used by commercial CAD software. We are also provided by a set of inspection paths γ_j, $j = 1, \dots, n$. For the simplicity of the argument, it is further assumed that each inspection path γ_j is fully contained in one of the boundary surfaces Γ_i, $\gamma_j \subset \Gamma_i$, i.e., the inspection path does not cross the creases of O. Therefore the surface normal field along each inspection path is assumed to be at least C^1-continuous. The orientation of the stylus along each path is treated separately, therefore the indices of the path and the boundary surface are omitted from now on, and the problem-to-be-solved is formulated as follows:

Inclination problem: Given a contact path $\gamma(t)$, $t \in [0, 1]$, and a to-be-inspected boundary surface patch Γ, such that $\gamma(t) \in \Gamma$ for all $t \in [0, 1]$. Find a fixed direction $\boldsymbol{d}$, $\boldsymbol{d} \in \mathbb{R}^3$, such that the constraints (1-3) defined above hold for any parameter $t \in [0, 1]$.

Remark 2. The parametrization of the inspection path $\gamma(t)$ can be seen as time (or pseudo-time), i.e., $\gamma(0)$ is the start point and $\gamma(1)$ is the end point in the case of an open curve, $\gamma(0) = \gamma(1)$ in the case of a closed curve. One can consider other parametrizations (e.g. arc-length) as well, but as will be seen later in Section 3.3, we set the number of parameter samples such that we guarantee a stable computation of the directions.

In the presented discrete setup, γ is given as a very fine polyline, i.e, an ordered set of measuring points — centers of the probe ball, shown in Fig. 7, (b) and (c).

3.2. Admissible stylus orientations

In order to find an admissible stylus orientation, three main objectives need to be met: inspection quality, physical feasibility, and rotation elimination. The objectives are now discussed in more detail.

3.2.1. Inspection quality

A probe stylus direction d, that allows for the best possible accuracy of the measurements, should span an angle between 60° and 75° with respect to the surface normal at the inspection point. Without loss of generality, one can assume that d is a unit vector. Then, at a fixed inspection point $\boldsymbol{c}^{\perp}$, a locus of admissible directions (seen as points on a unit sphere) corresponds to a spherical strip S, delimited by two circular cones sharing the same symmetry axis aligned with the surface normal at the point contact, one with the apex angle 75°, and the other with 60°, see Fig. 3.

Since the alternation of the probe's tilt is a slow procedure, compared to the movement of the three translational axes of the CMM's bridge, and in general is also less accurate, this work aims to find a constant direction of the stylus, if exists, in the CMM coordinate system along the whole inspection path. The desired direction d will point towards the intersection of the spherical strips associated with the possible stylus directions at every measurement point. For two inspection points, the corresponding intersection Ω is shown in orange in Fig. 3(b). To get a direction d that satisfies the first constraint throughout the inspection path γ, one needs to intersect all the spherical strips that correspond to every contact point of the inspection path, i.e.,

$$\Omega = \bigcap_{\gamma} S(\boldsymbol{c}^{\perp}) \approx \bigcap_{i=1}^{N} S_i. \tag{1}$$

Since this development works with a discrete set of inspection points, one considers a finite set of the spherical strips (right-hand side of Eq. (1)), that approximates the intersection of the (theoretically infinitely many) strips along smooth γ. The resulting intersection is computed numerically, the numerical issues are discussed in Section 3.3.

3.2.2. Physical feasibility

Once a set of candidate directions Ω is computed, global collisions of the kind *stylus–surface* need to be tested to select $\overline{\Omega}$, $\overline{\Omega} \subset \Omega$, which corresponds to the stylus orientations that are physically feasible, i.e., globally collision-free.

This stage incorporates numerical methods, in particular, for sampling the domain Ω, for which the libraries Trimesh [19] and Gmsh [20] are used, alongside with the standard libraries for Python3.

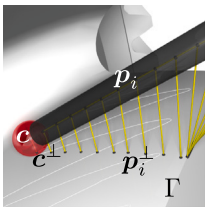

Fig. 4. Sampling the probe's axis to detect collisions.

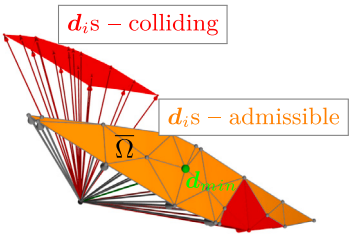

Fig. 5. Sampling the admissible orientation domain Ω by remeshing it in order to apply the collision detection test. Note that Ω is a part of a unit sphere, and has two disconnected components here, symmetric with respect to some plane. One component returns only colliding directions (further away, and therefore smaller, shown in red), while the second one (closer to the viewer, and therefore seemingly larger) offers both colliding and collision-free directions (orange $\overline{\Omega}$). The green point is the best orientation (see Section 3.3.1). (For interpretation of the references to color in this figure legend, the reader is referred to the web version of this article.)

For the collision detection procedure, a simplified geometrical representation of the probe was used, a ball tip with radius $r = 1$ mm connected to a stem, a cylinder with radius $r_s = 0.7$ mm and longer than the longest dimension of the model (the developed algorithm also allows for a variable diameter of a stem along its axis, in case its geometrical configuration is crucial for a particular workpiece). The collision detection procedures for the ball tip (sphere) and the stem (cylinder) were separated, see Fig. 4. Since the contact-based inspection methods require that the ball tip touches the surface, and the sensors register the touchdown within some tolerance δr, the event of an unwanted collision of the ball and the surface is realized when the shortest distance of the tip center to the model surface is less than $\|c - c^{\perp}\| < (r - \delta r)$.

On the other hand, the stem should not touch the inspected object O under any circumstances.To avoid such a collision, it is sufficient to sample the stem's axis and calculate the shortest distances of the sampled points (p_i) to the inspected surface patch Γ, see Fig. 4; the non-colliding points must fulfill $\left\|p_i - p_i^{\perp}\right\| \equiv d_{\text{stem},i} < r_s \,\forall i$; here i refers to the index of the sampling points on the stem's axis. In the developed implementation, stem is considered as a cylinder, even though its shape is slightly conical. The radius of the maximum sphere inscribed to the truncated cone is taken in the collision detection test.

3.3. Numerical computation of $\overline{\Omega}$

The region of candidates directions Ω is computed by Eq. (1), and one needs to eliminate colliding directions, i.e., to construct $\overline{\Omega}$. The described procedure can be rather heavy in terms of computing times, especially with finer model meshes, that is why, when sampling the admissible directions for the collision detection, it is needed to keep balance between the accuracy of the approach and the speed of calculations.

After computing Ω via Eq. (1), Ω is represented as a spherical mesh and is sampled via remeshing (with various max mesh-edge lengths), taking the vertices as sampling directions, see Fig. 5. Then, for each candidate direction $\boldsymbol{d}_i$, $\boldsymbol{d}_i \in \Omega$, the collision detection test at every point of the inspection path was applied (colliding domain is shown in red in the figure). The candidate directions that pass the test form $\overline{\Omega}$ (gray vertices in the figure) form a union of directions that meet the quality inspection constraint and guarantee positions of the stylus that are globally collision-free throughout the inspection path.

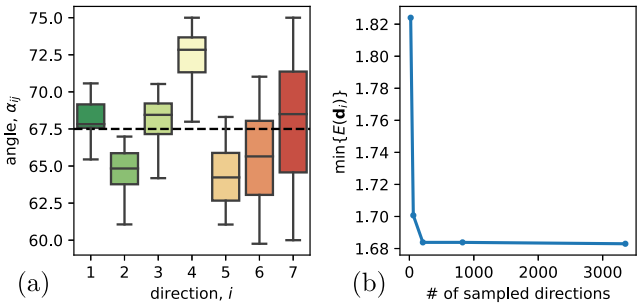

Fig. 6. (a) Boxplot (variances) of the stylus — surface normal angles (in degrees) changes along the inspection path for every sampled direction i. The best direction (green) has the most narrow box (smallest angular variation). If the preference is the least deviation from the center of the angular range, 67.5°, the best direction would be #3. (b) Best (lowest) variance achieved in Eq. (2) depending on the number of vertices of Ω. The computation gets stable for card(Ω) ≈ 100. (For interpretation of the references to color in this figure legend, the reader is referred to the web version of this article.)

3.3.1. Selection of optimal orientations

By now, the developed algorithm returns a set of directions that meet the quality inspection constraint along the whole inspection path and correspond to positions of the stylus that are globally collision-free throughout the inspection path. However, by fixing globally the inclination of the stylus and moving it along the inspection path, the angle between the stylus direction and the surface normal at the contact point varies (but remains within 60° to 75°, by construction) and one may ask what is the best direction, in a certain sense, among all the physically possible solutions.

One option is to look for a direction for which the variance $E_i := E(\boldsymbol{d}_i)$ of angles α_{ij} along the trajectory is the lowest. To this end, one can define a total angular variance in the least square sense, i.e.,

$$E(\boldsymbol{d}_i) = \frac{1}{N}\sum_{j=1}^{N}\left(\alpha_{ij} - \bar{\alpha}_i\right)^2, \tag{2}$$

where N is the number of samples on the inspection path, $\boldsymbol{d}_i$, $\boldsymbol{d}_i \in \overline{\Omega}$, is a candidate direction, i enumerates the sampled directions in $\overline{\Omega}$, $\bar{\alpha}_i = 1/N \sum_{j=1}^{N} \alpha_{ij}$ is the mean angle along the path. The best candidate direction, $\boldsymbol{d}_{min}$, that minimizes (2), is shown in green in Fig. 5.

Alternatively, one can look for minimum variance not from the mean value of the angle, but from the middle value of the interval that safeguards the inspection quality. In that case, one just replaces $\bar{\alpha}_i = 67.5$ in Eq. (2).

For the example shown in Fig. 5, it was also experimented with various sampling densities of the mesh Ω, ranging from tens to several thousands of vertices, using the Python remeshing routine. Fig. 5 shows the coarsest sampling level, where Ω consisted of 39 vertices (candidate directions), 21 being globally collision-free with the gear geometry throughout the inspection path. These points formed $\overline{\Omega}$ (orange) and the best direction was computed via Eq. (2).

Fig. 6(a) shows a boxplot of the angular variation for the top 7 directions, the dark green box being the best one which corresponds to $\boldsymbol{d}_{min}$ in Fig. 5. Fig. 6(b) shows the computation of the minimizer of Eq. (2) as a function of the number of vertices of Ω. For large number of vertices (card(Ω) > 100), the value of the minimizer became almost unchanged, and the same holds also for the corresponding vector $\boldsymbol{d}_{min}$. From this experiment, one concludes that setting card(Ω) = 100 is sufficient for a stable computation of $\boldsymbol{d}_{min}$ and this value was set as default in the developed algorithm.

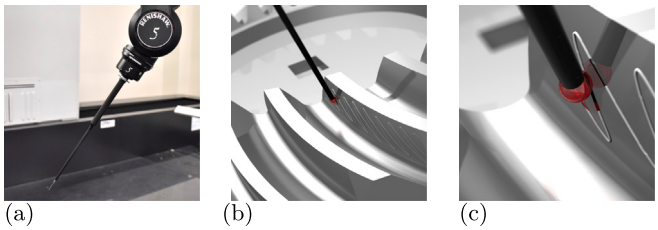

Fig. 7. (a) Probe setup used in the simulations; inspection path, i.e., the trajectory that the probe tip should move along. A general view (b) and a zoomed view (c) are shown.

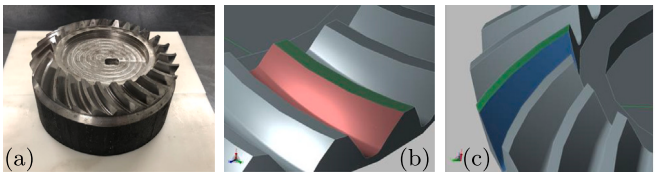

Fig. 8. A to-be-inspected workpiece. (a) A manufactured spiral bevel gear. The to-be-inspected surfaces are (b) the top land (green) and right flank (red), and (c) left flank (blue). (For interpretation of the references to color in this figure legend, the reader is referred to the web version of this article.)

4. Physical validations and results

The presented algorithm is developed to be applied to both simple and complex geometries. In order to be validated, the proposed (3+2)-axis inspection method was applied to three surfaces on a spiral bevel gear. The obtained measurements were analyzed and compared to conventional 3-axis and 5-axis inspection methods.

4.1. Case study: A tooth of spiral bevel gear

The selected case study consists of a tooth of a spiral bevel gear shown in Fig. 7. The selected geometry meets two main inspection challenges: surface complexity and global accessibility. From the complexity point of view, spiral bevel gear teeth are known as complex surfaces to be manufactured and inspected. In terms of global collision detection, the gear geometry is also challenging due to the proximity of the neighboring tooth, that gives non-trivial collision constraints. For this case study, three different inspection methods were performed and the dimensional deviation results were compared: 3-axis inspection, 5 continuous axes inspection and (3+2) axis proposed inspection method.

The real measurements were conducted on a 5-axis CMM, Mitutoyo Crysta Apex S-162012, recall Fig. 1. The parameters of the selected machine are shown in Table 1. The maximum Permissible error (MPE) for this measuring machine is defined as:

$$MPE = 4.5\mu m + 5.5 \cdot 10^{-3} L \tag{3}$$

where L is the length of the measurements in millimeters. The MAE is the maximum deviation that the CMM commits when it measures a path of length L. During the measurements, the 5-axis inspection head REVO-2 (by Renishaw) was used.

The tool used consists of the RSH350 stem and the M2 STY DR2 L20 EWL14 D1.4SS stylus. The stem is carbon fiber with a length of 254.3 mm (without the stylus) while the stylus has a 2 mm diameter synthetic ruby sphere. Finally, the probe used is the RSP2, which can measure continuously in 2D (x, y) and perform 3D contact trigger measurements (x, y, z). The points have been measured continuously using a speed of 5 mm/s. The pitch between points was set to 0.01 mm.

In the measurements, the inspection paths were generated from the inspection points using the *Sweep Scan* command. This command defines a sinusoidal contour on the to-be-inspected surface Γ (see Fig. 9) using control points (blue).

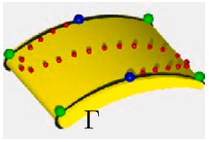

Fig. 9. *Sweep Scan* command. (For interpretation of the references to color in this figure legend, the reader is referred to the web version of this article.)

Table 1
The parameters of Mitutoyo Crysta Apex S-162012.

		Cysta Apex S-162012
Axis		5 (X, Y, Z, A, B)
Work range	X Axis	1,600 mm
	Y Axis	2,000 mm
	Z Axis	1,200 mm
	A Axis	-5° / 120°
	B Axis	±180°
Max. workpiece height		1,400 mm
Max. weight on the worktable		3,500 kg
Resolution		0.1 µm
Software		MCOSMOS v4.2R3

Table 2
The optimal unit directional vectors (coordinate-wise) for each flank, computed by our algorithm described in Section 3.

	d_x	d_y	d_z
Upper land	−0.10324	−0.98594	0.13142
Right flank	0.04544	−0.93882	−0.34140
Left flank	0.66224	−0.72842	−0.17561

Each control point requires two additional points (green) that define the maximum and minimum of the amplitude of the sinusoid. For the definition of the sinusoid, a step of 2 mm has been used.

To define the inspection path, one sets a set of control points that roughly indicate the desired inspection path, see Fig. 10. These control points were selected such that the wavelength of the sinusoidal path is 2 mm and a distance between two neighboring inspection points (red dots in Fig. 9) is less than 0.1 mm. For the upper land that is flatter, four set of triplets of inspection points were selected. In the case of curved flanks and the path should be longer, five sets of points were selected.

With the Sweep Scan command, one generates sinusoidal inspection trajectories by setting a few positions (blue dots) and tangent directions (green dots), see Fig. 9. Using the inspection software MCOSMOS v4.2R3 by Mitutoyo, one can also specify the number of amplitudes. The set of points shown in Fig. 10 generates inspection path later show Fig. 11.

4.2. Results: Comparison of measuring strategies

In order to validate the proposed 3+2 optimized inspection path, three different physical validations were performed: (1) 5 continuous axes inspection *(variable)*, (2) 3-axis conventional inspection *(3-axis)* and (3) Optimized 3+2 inspection *(3+2 Optimized)*. On the one hand, obtained results were analyzed to estimate the measuring deviations related to expected geometry. Considering the 5-axis strategy as the most accurate one, the deviation of the other ones was calculated.

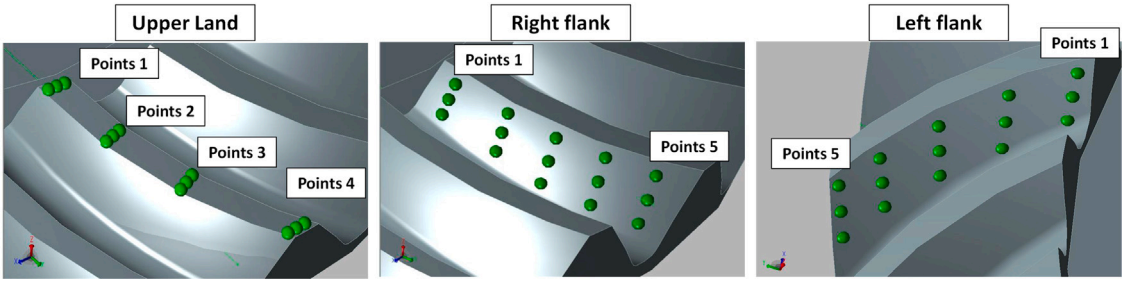

		Minimum	Middle	Maximum
Point 1	X / mm	12.180	13.494	14.807
	Y / mm	74.013	73.865	73.711
	Z / mm	20.695	20.649	20.592
Point 2	X / mm	8.461	9.760	11.058
	Y / mm	82.351	82.581	82.807
	Z / mm	16.111	15.892	15.664
Point 3	X / mm	1.957	3.300	4.643
	Y / mm	91.298	91.787	92.271
	Z / mm	11.079	10.769	10.450
Point 4	X / mm	-10.088	-8.513	-6.937
	Y / mm	102.385	102.534	102.676
	Z / mm	4.264	4.260	4.246

		Minimum	Middle	Maximum
Point 1	X / mm	16.543	16.196	15.690
	Y / mm	73.127	73.944	74.701
	Z / mm	12.097	14.845	17.587
Point 2	X / mm	13.148	12.849	12.369
	Y / mm	80.703	81.412	82.021
	Z / mm	7.270	10.650	14.028
Point 3	X / mm	9.4538	9.109	8.539
	Y / mm	86.4136	87.368	88.163
	Z / mm	2.457	6.4533	10.487
Point 4	X / mm	4.708	4.379	3.856
	Y / mm	92.189	93.117	93.872
	Z / mm	-1.1172	3.097	7.324
Point 5	X / mm	-0.6128	-1.105	-1.758
	Y / mm	97.140	98.229	99.138
	Z / mm	-4.682	-0.449	3.804

		Minimum	Middle	Maximum
Point 1	X / mm	5.169	7.198	9.372
	Y / mm	73.627	74.297	74.982
	Z / mm	10.790	14.422	17.967
Point 2	X / mm	0.294	2.606	5.042
	Y / mm	80.851	81.872	82.922
	Z / mm	5.531	9.366	13.113
Point 3	X / mm	-5.118	-3.028	-0.867
	Y / mm	87.852	89.275	90.728
	Z / mm	1.801	5.149	8.439
Point 4	X / mm	-11.138	-9.091	-7.005
	Y / mm	93.815	95.455	97.118
	Z / mm	-1.328	1.831	4.953
Point 5	X / mm	-16.768	-14.458	-12.131
	Y / mm	98.051	99.724	101.411
	Z / mm	-3.051	-0.551	2.648

Fig. 10. Inspection points. On each of the inspected parts of the gear tooth, a set of inspection points was selected; from left to right: upper land, Right flank, and Left flank. On the flat upper land it was selected $n = 3 \times 4$ inspection points (green), while on the curved parts of the left and right flanks we increased it to $n = 3 \times 5$ points. Bottom row: the coordinates of the corresponding sets of inspection points. (For interpretation of the references to color in this figure legend, the reader is referred to the web version of this article.)

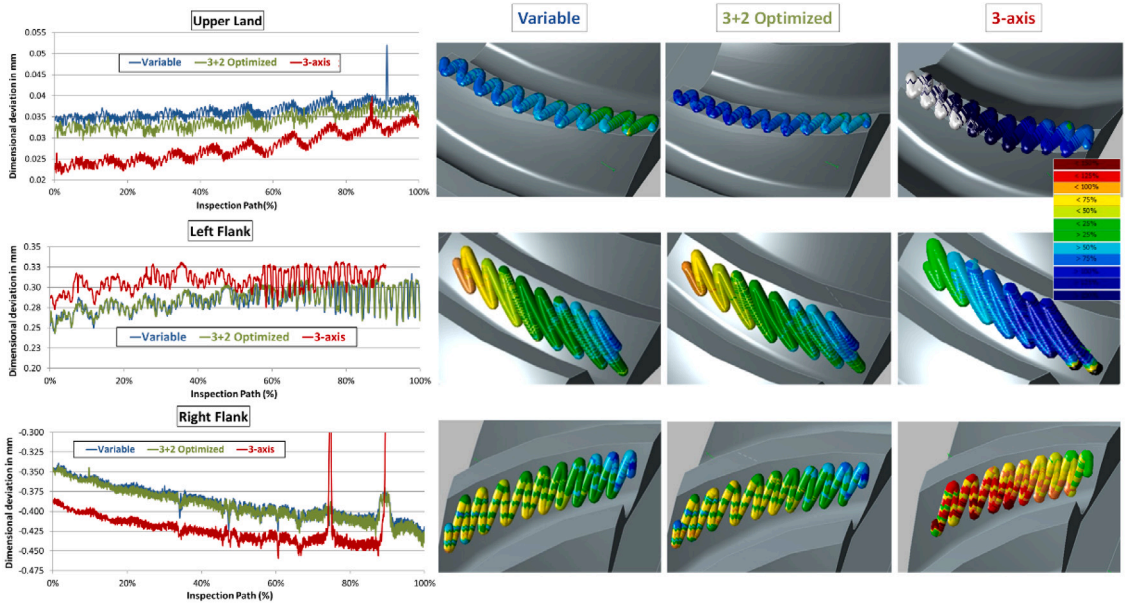

Fig. 11. Inspection deviations. Each row shows the deviation for the inspected surface; from top to bottom: upper land, right flank, and left flank. The first column shows the inspection deviation throughout the inspection path, measured in mm, for a variable stylus orientation (blue) computed by the commercial software MCOSMOS, and the constant orientation computed by the presented algorithm (red). The middle and right columns show the deviation distribution throughout the 3D inspection path, color-coded by the measurement accuracy. The accuracy color bar is showed framed. The color-coding represents the deviation (expressed as a percentage) where the minimum deviation gets mapped to −100% while the maximum deviation to +100%. In the case of undercutting (upper land and right flank, both extremal values are positive), the most accurate measurements correspond to dark blue color, while for the overcutting (left flank, both extremal values are negative), the most accurate measurements correspond to red. (For interpretation of the references to color in this figure legend, the reader is referred to the web version of this article.)

Performed physical validations analyze three test surfaces (upper land and the two flanks) of a tooth of spiral bevel gear shown in Fig. 8. The first test uses variable stylus orientations and the second test uses 3+2 strategy computed by MCOSMOS software. The third one, however, uses constant stylus orientations computed by the presented algorithm described in Section 3, see Table 2. This table shows the coordinates of the unit probe direction vector d, i.e., the orientation cosines of the CMM.

On each surface, Fig. 11 shows the accuracy of each measurement and colormaps reflecting the measurement deviations. Hereafter, the obtained results of the measurements on the three surfaces are discussed in detail:

- *Upper land*: Variable measurement obtained a maximum dimensional deviation related to the nominal geometry of 0.04 mm, close to the optimized strategy that presented 0.037 mm of deviation from nominal. Finally, the 3-axis strategy presented a maximum deviation from nominal of 0.03 mm. Nevertheless, in Fig. 11 one can observe that the analyzing the variability along the entire path, for 3-axis the variability is higher due to the

less flexibility presented in the inspection path. It is worthy to mention that the magnitude of deviation from nominal is 35–40 micrometers, being the highest differences among the three strategies up to 10 micrometers. All three performed strategies achieved 100% path without collisions.

- *Right flank:* Variable measurements obtained a max. deviation from nominal of −0.425mm aligned to the ones obtained using the optimized strategy, whereas the 3-axis strategy presented a max. deviation from nominal of −0.46mm. In this case, the highest differences among the three strategies are up to 50 micrometers. Both the variable strategy and the optimized one covered the 100% of the surface, the 3-axis strategy, however covered only 89.85% of the surface before suffering a collision.
- *Left flank:* Variable measurements obtained a max. deviation from nominal of 0.30 mm aligned to the ones obtained using the optimized strategy. However, the 3+2 strategy presented a max. deviation from nominal of 0.34 mm. In this case, the highest differences among the three compared strategies went up to 40–50 micrometers. Both the variable strategy and the optimized one covered the again the whole 100% of the surface, while the 3-axis strategy covered only 90.72% of the surface before suffering a collision.

Analyzing obtained results for each strategy, for upper land geometry, the differences are negligible due to the simplicity of the surface to be measured. Nevertheless, the complexity presented on the right and left flanks led to the necessity of a higher accuracy and flexible strategy. At this point, 5-axis inspection is the one that presented optimal deviation results, closely followed by the optimized strategy. Finally, the 3-axis could not complete the entire path for right and left flank without a collision.

In summary, three inspection strategies were applied along the inspection path on three surfaces of a spiral bevel gear. The variable strategy and the 3+2 optimized one performed rather similarly. The 3 axis strategy performed considerably worse. Considering the 5-axis strategy as a reference, the dimensional deviation errors committed by the proposed strategy and the 3-axis strategy were calculated. For this purpose, an average of obtained results was performed along the three different surfaces and a relative error was calculated with respect to the variable strategy following the expression (4). The Relative Error (RE) is defined as:

$$RE = \frac{1}{n}\sum_{i=1}^{n}\frac{y_i - x_i}{x_i}100 \tag{4}$$

where x_i are dimensional deviations from nominal values using the 5-axis strategy and y_i values correspond to 3+2 optimized strategy and 3-axis strategy. For the 3+2 optimized one, the relative errors reached 6.5% for upper land, 0.64% for the right flank, and 0.15% for the left flank, respectively. However, for the 3 axis strategy, the relative errors were up to 23.83% for upper land, 8.27% for the right flank, and 8.22% for the left flank.

4.3. Discussion & limitations

Global collision detection. In the developed stylus motion planning algorithm, it was tested the case that the cylindrical part of the probe collides with the gear geometry. Similarly to the collision test in [21], the tool's axis is conceptualized as a cylinder, sampled, and the distance to the gear geometry (subtracted by the cylinder's radius) served as a simple collision test. It was assumed that the stylus is sufficiently long compared to the reference geometry, which indeed was the case. For a shorter stylus (or larger geometry) one should consider collision of the upper (support) part of the inspection machine in the collision detection test.

Alternative objects to inspect. The proposed algorithm was demonstrated on a tooth of spiral bevel gear due to the challenges presented by its geometry, however, majority of the algorithm is generic and could be applied to other curved geometries as well. The only issue is the existence of a non-empty $\overline{\Omega}$ that contains the physically feasible directions. If $\overline{\Omega}$ is empty, in order to get some candidate directions, one could release the angular constraint on stylus orientation with the reference to the surface normal, and then look for a solution that violates the constraints the least, in the least squares sense. If the collision test fails for all the candidate directions, it would be concluded that there is no constant probe orientation. Such a scenario can occur, e.g., for surfaces with cavities, where the existence of a single probe orientation would be hardly possible. It was intentionally used a tooth of spiral bevel gear that implies complex surfaces along with accessibility issues. However, the proposed algorithm is not affected by the accuracy of the manufacturing and can be used also for highly-accurate workpieces, e.g. those from [22].

Inspection machines. The presented results show a potential alternative to 3D free-form surfaces inspection using only 3-axis machines. It should be highlighted that the accuracy obtained through the (3+2) algorithm is comparable to the 5-axis, offering, at the same time, higher accuracy than conventional 3-axis inspection. Additionally, it is avoided the use of the two extra rotational axes. The requirement of the rotary axis is just for initial positioning, but not during the measuring process. Consequently, the measurements can be accomplished on simpler machines, involving resources minimization (affordable measuring tools) and more user-friendly programming systems that requires qualification only for 3-axis machines instead of 5-axis.

Machine inertia. In the performed physical experiments, the speed of the inspection machine was set intentionally low to avoid measurement inaccuracies caused by the machine inertia. Therefore, the inspection times could not be assessed, being almost the same for the approach using a variable probe orientations (5-axis inspection) and this innovative method with constant probe orientations (3-axis inspection).

5. Conclusion

A new 3+2 path-planning strategy for inspection of free-form surfaces has been introduced, and demonstrated on the test case of a tooth of a spiral bevel gear. The inspection path is given as an input and the developed optimization framework looks for an orientation of the inspection probe such that the stylus angle is within a given threshold with respect to surface normal at the inspected points, the position of the probe is globally collision-free, and the orientation direction is constant — throughout the inspection path. The presented algorithm was physically validated, demonstrating that the approach outperforms the Mitutoyo's software MCOSMOS in terms of the inspection deviation.

The present work reaches to the following conclusions:

- Comparing the three measuring strategies, the 5-axis strategy is the most accurate one, followed closely by the proposed 3+2 algorithm. So, the present algorithm allows the use of only 3-axis inspections through 3+2 machines, that implies a financial advantage compared to more expensive 5-axis inspection machines.
- Simple surfaces, such as upper land, could be measured using any of the three strategies accomplishing the 100% of the programmed surface. Moreover, the highest differences presented in these results are up to 10 micrometers.
- Free-form surfaces or complex surfaces with limited accessibility, such as right and left flanks, presented some difficulties for 3-axis strategy to accomplish the entire programmed surfaces, warning a collision error at 89.85% and 90.72% along the path, respectively. It is concluded that the 3-axis strategy is not adequate to measure these type or surfaces, due to the strategy flexibility limitations.

As a future research thread, it is aimed at path optimization as the current setup keeps the given inspection path, which is suboptimal. One may look for optimized trajectories that, for example, would be more convenient for the inspection machine from the kinematics perspective and, consequently, could further address the challenge of reducing the inspection time.

Declaration of competing interest

The authors declare that they have no known competing financial interests or personal relationships that could have appeared to influence the work reported in this paper.

Acknowledgments

This work was supported by the European Union's Horizon 2020 program under grant agreement No 862025, the Spanish Ministry of Science, Innovation and Universities, grant No PID2019-104488RB-I00, BCAM "Severo Ochoa" accreditation (SEV-2017-0718), and by the Elkartek funding program, grant no. KK-2020/00102. Michael Bartoň was supported by the Ramón *y* Cajal fellowship RYC-2017-22649.

References

[1] Hocken RJ, Pereira PH, et al. Coordinate measuring machines and systems. Vol. 2. CRC press Boca Raton; 2012.
[2] Alessandro V, Gianni C, Antonio S. Axis geometrical errors analysis through a performance test to evaluate kinematic error in a five axis tilting-rotary table machine tool. Precis Eng 2015;39:224–33.
[3] Sładek JA. Coordinate metrology. In: Accuracy of systems and measurements. Springer; 2016.
[4] Pfeifer T, Spur G. Task-specific gauge for the inspection of coordinate measuring machines. CIRP Ann 1994;43(1):465–8.
[5] Suh S, Lee E, Kim H, Cho J. Geometric error measurement of spiral bevel gears using a virtual gear model for STEP-NC. Int J Mach Tools Manuf 2002;42(3):335–42.
[6] Lin C-H, Fong Z-H. Numerical tooth contact analysis of a bevel gear set by using measured tooth geometry data. Mech Mach Theory 2015;84:1–24.
[7] Wang S, Zhou Y, Tang J, Tang K, Li Z. Digital tooth contact analysis of face gear drives with an accurate measurement model of face gear tooth surface inspected by CMMs. Mech Mach Theory 2022;167:104498.
[8] Lu X, Zhao X, Hu B, Zhou Y, Cao Z, Tang J. A measurement solution of face gears with 3D optical scanning. Materials 2022;15(17):6069.
[9] Li T, Li J, Deng X, Yang J, Li G, Ma W. A new digitized reverse correction method for hypoid gears based on a one-dimensional probe. Meas Sci Technol 2017;28(12):125004.
[10] Pisula J. The geometric accuracy analysis of polymer spiral bevel gears carried out in a measurement system based on the Industry 4.0 structure. Polimery 2019;64(5):353–60.
[11] Liu R, Zhong D, Lyu H, Han J. A bevel gear quality inspection system based on multi-camera vision technology. Sensors 2016;16(9):1364.
[12] Urbas U, Zorko D, Černe B, Tavčar J, Vukašinović N. A method for enhanced polymer spur gear inspection based on 3D optical metrology. Measurement 2021;169:108584.
[13] Gonzalez-Perez I, Fuentes-Aznar A. Reverse engineering of spiral bevel gear drives reconstructed from point clouds. Mech Mach Theory 2022;170:104694.
[14] Zhou Z, Zhang Y, Tang K. Sweep scan path planning for efficient freeform surface inspection on five-axis CMM. Comput Aided Des 2016;77:1–17.
[15] ElKott DF, Veldhuis SC. Isoparametric line sampling for the inspection planning of sculptured surfaces. Comput Aided Des 2005;37(2):189–200.
[16] Zhou A, Guo J, Shao W. Automated inspection planning of freeform surfaces for manufacturing applications. In: 2011 IEEE international conference on mechatronics and automation. IEEE; 2011, p. 2264–9.
[17] Ainsworth I, Ristic M, Brujic D. CAD-based measurement path planning for free-form shapes using contact probes. Int J Adv Manuf Technol 2000;16(1):23–31.
[18] Li Y, Zeng L, Tang K, Xie C. Orientation-point relation based inspection path planning method for 5-axis OMI system. Robot Comput-Integr Manuf 2020;61:101827.
[19] Dawson-Haggerty, et al. trimesh. 2019, URL https://trimsh.org/. 2019-12-8.
[20] Geuzaine C, Remacle J-F. Gmsh: A 3-D finite element mesh generator with built-in pre-and post-processing facilities. Internat J Numer Methods Engrg 2009;79(11):1309–31.
[21] Bartoň M, Bizzarri M, Rist F, Sliusarenko O, Pottmann H. Geometry and tool motion planning for curvature adapted CNC machining. ACM Trans Graph 2021;40(4).
[22] Escudero GG, Bo P, González-Barrio H, Calleja-Ochoa A, Bartoň M, de Lacalle LNL. 5-axis double-flank CNC machining of spiral bevel gears via custom-shaped tools—Part II: physical validations and experiments. Int J Adv Manuf Technol 2022;119(3-4):1647–58.